HELICOPTER ROTOR WAKE DISTORTION MODELS FOR MANEUVERING FLIGHT

J.V.R. Prasad Jinggen Zhao
Professor Graduate Student
School of Aerospace Engineering
Georgia Institute of Technology
Atlanta, GA, USA

David A. Peters
Professor
Department of Mechanical Engineering
Washington University
St. Louis, MO, USA

Abstract

A new model for the dynamic wake distortion effects for maneuvering and transitioning from forward flight is developed in this paper. The associated time constants of the model are extracted using results from the vortex tube analysis. The new model is integrated with a generic helicopter flight simulation model. Correlations with the Black Hawk helicopter flight test data are used to study the effect of wake distortion terms on simulation fidelity for maneuvering flight. Also, analytical and numerical comparisons are made between the new model and the augmented dynamic wake distortion inflow model previously proposed in the literature.

Nomenclature

C_T, C_L, C_M	rotor thrust, rolling moment and pitching moment coefficients
$[C]$	matrix of inflow coupling parameters for wake curvature
$[C_{pk}]$	wake curvature inflow coupling parameter matrix terms
K_{R}	wake distortion parameter
K_{Re}	wake curvature parameter
$[L]$	induced inflow coefficient matrix
$[M]$	apparent mass matrix
$\overline{p}, \overline{q}$	non-dimensional roll and pitch rates
v_h	mean inflow across rotor disc in hover
$[V]$	mass flow parameter matrix
$\mathrm{V_c}$	nondimensional normal component of free stream inflow
V_m	mean inflow parameter
$\overline{V}$	inflow parameter for the first harmonic inflow states
X	wake skew state
Ω	rotor rotational speed
α_j^r, β_j^r	rotor induced inflow coefficients
β_{1c}, β_{1s}	longitudinal and lateral tilts of tip-path plane
χ	wake skew angle
κ_c, κ_s	longitudinal and lateral wake curvatures
μ	advance ratio
λ_0	nondimensional mean inflow
λ_i	nondimensional mean induced inflow
$\Delta\lambda_{1c}$	nondimensional longitudinal inflow gradient due to wake distortion
$\Delta\lambda_{1s}$	nondimensional lateral inflow gradient due to wake distortion
τ_R, τ_X, τ_S	time constants associated with wake bending, wake skew and wake spacing dynamics
$[\tau_D]$	time constant matrix associated with wake distortion dynamics
$\tau_{\mathrm{n}}^{\mathrm{mc}}, \tau_{\mathrm{n}}^{\mathrm{ms}}$	forcing functions in the generalized dynamic wake model

Paper presented at the 28th European Rotorcraft Forum, Bristol, UK, September 17-20, 2002.

Introduction

High fidelity representation of the rotor wake effects is an important ingredient in helicopter aeromechanics and flight dynamics analysis. It is well recognized in recent years that the wake distortion effects are the primary source of the off-axis response behavior observed in maneuvering flight. Several methods have been proposed to model wake distortion effects using simple empirical corrections to comprehensive CFD models. Some of the empirical approaches proposed to correct the off-axis predictions are very limited in scope and, in general, they are not applicable to the entire flight envelope. Comprehensive CFD calculations are computationally expensive and therefore they are not suitable for flight simulation and control law development applications. In contrast, the finite state dynamic inflow models developed in the late 80's (Refs. 1, 2), which are routinely used in rotorcraft industry, can be easily combined with other aeromechanics and flight dynamic models for stability and control analysis and for real-time simulation purposes.

When helicopters transition through different flight conditions, the rotor wake also transitions through different shapes. The wake distortions due to pitch/roll

maneuvers have been recognized to significantly contribute to the experimentally observed off-axis response to control inputs. Previous investigations (Refs. 3 ~ 9) of this problem have assumed a quasi-steady rotor wake model, which assumes that the wake bending due to rotor pitch and/or roll rates takes place instantaneously at each time instant. However, as pointed out in Refs.10~12, it does take some finite time to develop the wake curvature in reality. Hence, it is imperative that an evaluation of the wake distortion dynamics during transitional flight is carried out for the development of high fidelity simulation models and control law development.

It is fairly certain that the dynamic wake distortion effects are aerodynamic in nature and hence, they can be captured using aerodynamic principles. Several aerodynamic tools, from simple momentum theory to comprehensive free wake methods, have emerged in the literature to study rotor wake distortion effects during maneuvering flight. In Refs.11 and 12, a free wake method is used to calculate the time-dependent nature of the inflow gradient on an isolated model rotor undergoing either step pitching velocity or step advance ratio changes from hover. An important finding of Refs. 11 and 12 is that the variation of the inflow gradient exhibits a first order behavior with time and hence, the time dependent nature of inflow variation may be approximated using first order equations. In Refs. 13 and 14, a new dynamic wake distortion model for helicopter maneuvering and transitional flight near hover condition was developed.

In this paper, the rotor dynamic wake distortion model for helicopter maneuvering and transitional flight near hover condition, developed in Refs. 13 and 14, is extended for modeling of rotor dynamic wake distortion effects in forward flight cases. The newly developed model is combined with the augmented Peters-He finite state inflow model (Ref. 9) and the augmented Pitt-Peters 3-state dynamic inflow model (Ref. 5). Analytical and numerical comparisons are made between the new model and the augmented dynamic wake distortion inflow model proposed by Keller et al (Refs. 4, 10) in order to clarify any differences between these two models. The new model is integrated into a generic helicopter flight simulation model and predicted responses to cyclic doublets in forward flight are compared with the Black Hawk helicopter flight test data.

Modeling of Dynamic Wake Distortion Using the Vortex Tube Method

In the vortex tube method, the vortices generated at the rotor blades are wrapped around a tube of continuous vorticity, representing the outer surface of the rotor wake. The induced inflow on the rotor disk due to the vortex tube can be calculated using the Biot-Savart Law. This method can be easily extended to the case of a rotor undergoing transient maneuvers, by prescribing the distorted wake geometries, which is equivalent to a dynamic vortex tube whose shape continuously changes with time.

In modeling of dynamic wake distortion effects near hover using the vortex tube method, Refs. 13 and 14 assume circumferentially uniform vortex tube strength as given by the mean rotor loading. For modeling of dynamic wake distortion effects in forward flight considered here, one should treat the vortex tube strength to be circumferentially varying as has been done in Ref. 15. However, the present study neglects the circumferential variation of vorticity and considers only the rotor mean loading in the vortex tube analysis.

Dynamic Wake Bending Effect in Forward Flight

A typical variation of the longitudinal inflow gradient over the rotor disk with time, predicted by the vortex tube analysis is shown in Fig. 1, for a nondimensional pitch rate of $\bar{q} = 0.005$ and thrust coefficient of $C_T = 0.0065$ at a forward flight of μ=0.05. Also superimposed in the plot is a first order approximation. It can be seen that the inflow gradient exhibits a first order behavior with time.

Figure 2 shows the values of the nondimensional time constant associated with the wake bending dynamics in forward flight (μ=0.05) corresponding to different values of thrust coefficient as extracted from the vortex tube analysis results. In Fig. 2, the symbols are those given by the vortex tube model and the solid line is an empirical approximation obtained as

$$\tau_R = \frac{32}{15\pi\overline{V}} \tag{1}$$

where $\overline{V}$ and V_m are given by

$$\overline{V} = \frac{\mu^2 + (2\lambda_i + V_c)(\lambda_i + V_c)}{V_m} \tag{2}$$

$$V_m = \sqrt{\mu^2 + (\lambda_i + V_c)^2} \tag{3}$$

It can be seen that the empirical formula (equation (1)) agrees well with the results predicted by the dynamic vortex tube model. For the hover case, equation (1) reduces to

$$\tau_R = \frac{16}{15\pi v_h} \tag{4}$$

where v_h denotes the nondimensional mean induced velocity in hover. Equation (4) matches with the result

given in Refs. 13 and 14 for the dynamic wake bending for the hover case.

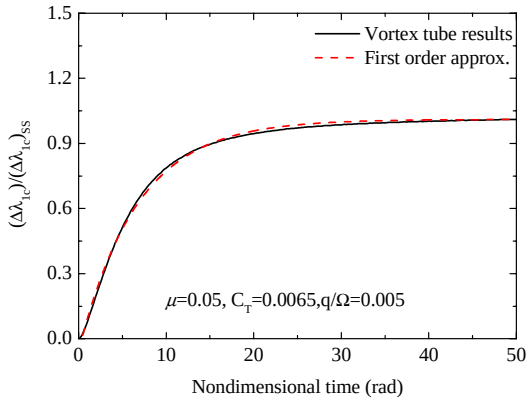

Figure 1. Inflow gradient growth with curvature effect for a four-bladed rotor in forward flight, μ=0.05, C_T=0.0065, $\bar{q} = 0.005$.

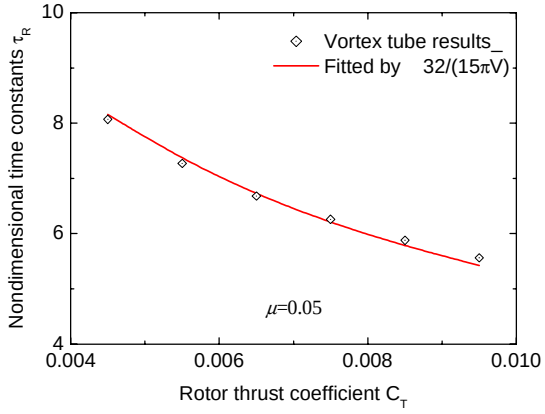

Figure 2. Variation of nondimensional time constant associated with wake curvature effect versus rotor thrust coefficient in forward flight, μ=0.05.

Dynamic Wake Skew Effect in Forward Flight

Figure 3 shows the variation of rotor inflow gradient with time to a step advance ratio of $\Delta\mu = 0.01$ from forward flight (μ=0.05) at a thrust coefficient of $C_T = 0.0065$, predicted using the vortex tube method. It can be seen that the inflow gradient once again exhibits a first order variation with time. Figure 4 shows the values of the nondimensional time constant associated with the dynamic wake skew effect in forward flight for different values of thrust coefficient as extracted from the vortex tube analysis results. In Fig. 4, the symbols are the results predicted by the dynamic vortex tube model and the solid line is an empirical approximation obtained as

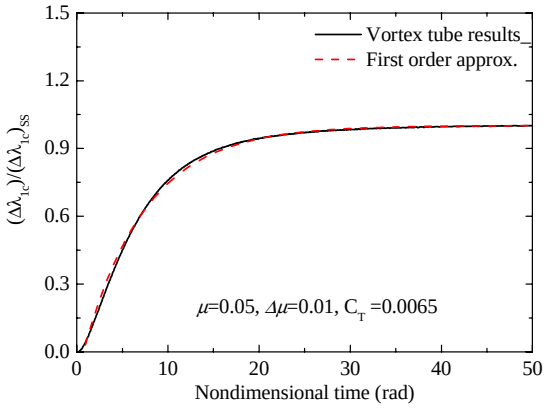

Figure 3. Inflow gradients across the rotor disk plane due to a step advance ratio from forward flight, μ=0.05, C_T=0.0065, $\Delta\mu = 0.01$.

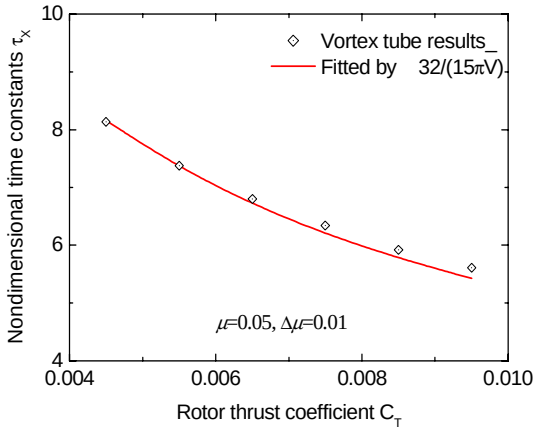

Figure 4. Variation of nondimensional time constant associated with dynamic wake skew effect with rotor thrust coefficient in forward flight, μ=0.05.

$$\tau_X = \frac{32}{15\pi\bar{V}} \tag{5}$$

It can be seen that the above formula agrees well with the results predicted by the dynamic vortex tube model. Therefore, it can be used to represent the time constant associated with the wake skew dynamics in forward flight. For the hover case, equation (5) reduces to

$$\tau_X = \frac{16}{15\pi v_h} \tag{6}$$

where v_h denotes the mean induced velocity in hover. Equation (6) matches with the result of Refs. 13 and 14 for the dynamic wake skew from hover.

Dynamic Wake Spacing Effect in Forward Flight

Figure 5 shows the variation with time of the mean induced inflow normalized by the inflow at hover for a step change in climb rate of $0.1v_h$ at a forward flight of μ=0.05, as predicted from the vortex tube method. It can be seen that the inflow growth exhibits a first order variation with time.

Figure 6 shows values of the nondimensional time constant associated with wake spacing dynamics in forward flight case for different values of rotor thrust coefficient as extracted from vortex tube analysis results. The solid line in Fig. 6 is an empirical approximation obtained as

$$\tau_S = \frac{32}{15\pi V_m} \tag{7}$$

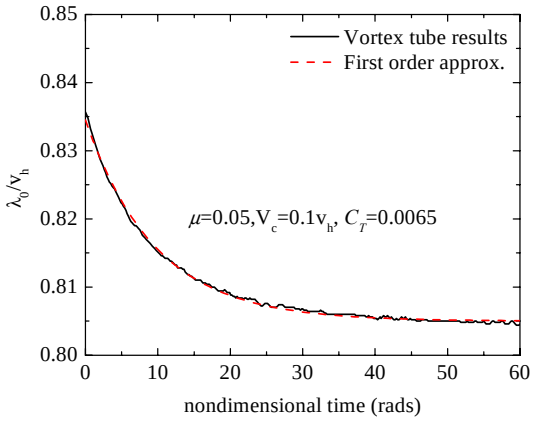

Figure 5. Mean induce inflow variation with time following a step climb rate, $V_c = 0.1v_h$ forward flight, μ=0.05

For the hover case, equation (7) reduces to

$$\tau_S = \frac{32}{15\pi v_h} \tag{8}$$

where v_h is the mean induced velocity in hover. It can be seen that equation (8) is consistent with the model for dynamic wake spacing effect near hover of Refs. 13 and 14.

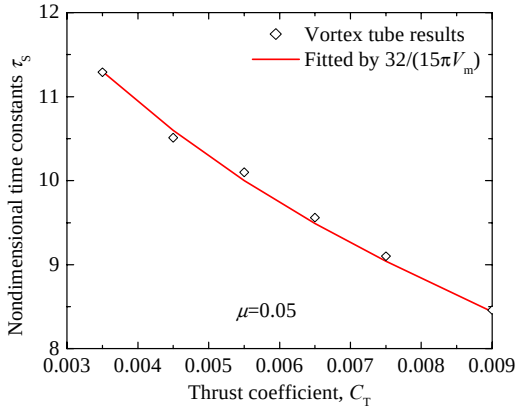

Figure 6. Nondimensional time constant associated with dynamic wake spacing effect vs. rotor thrust coefficient in forward flight case.

Dynamic Wake Distortion Model

It is clear from the vortex tube analysis in the previous section that the dynamic wake distortion effects, i.e., dynamic wake bending, skew and spacing effects, have significant influence on the rotor inflow during maneuvering and transitional flight phases where the rotor wake transitions through different shapes. The results given by the dynamic vortex tube model in the previous section show that the dynamic inflow variations due to dynamic wake bending, wake skew and wake spacing effects in forward flight conditions essentially exhibit first order behavior with time. Therefore, the dynamic wake distortion effects can be represented by a set of first order equations as

$$[\tau_D]\begin{Bmatrix} \dot{X} \\ \dot{S} \\ \dot{\kappa}_c \\ \dot{\kappa}_s \end{Bmatrix} + \begin{Bmatrix} X \\ S \\ \kappa_c \\ \kappa_s \end{Bmatrix} = \begin{Bmatrix} X \\ S \\ \kappa_c \\ \kappa_s \end{Bmatrix}_{qs} \tag{9}$$

where X, S, κ_c, κ_S are the wake skew, wake spacing, longitudinal and lateral wake curvatures, respectively. The matrix $[\tau_D]$ contains the time constants associated with the dynamic wake distortion effects. In general, the wake skew, wake spacing and wake curvature states are fully coupled in forward flight. However, the coupling effects between these states are neglected in the present study and the time constant matrix $[\tau_D]$ is assumed to be diagonal as

$$[\tau_D]=\begin{bmatrix}\tau_X & 0 & 0 & 0\\ 0 & \tau_S & 0 & 0\\ 0 & 0 & \tau_R & 0\\ 0 & 0 & 0 & \tau_R\end{bmatrix} \tag{10}$$

where τ_X, τ_S and τ_R are given by the empirical formulae (eqns. 5, 7 and 1, respectively) developed in the previous section from vortex tube analyses results.

The right-hand-side of equation (9) corresponds to the quasi-steady wake skew, spacing, longitudinal and lateral curvatures, which are be given by

$$\begin{aligned}(X)_{qs}&=\tan\left(\frac{\chi}{2}\right) \qquad (S)_{qs}=2\pi V_m\\ (\kappa_c)_{qs}&=\frac{\bar{q}-\dot{\beta}_{1c}}{V_m} \quad (\kappa_s)_{qs}=\frac{\bar{p}-\dot{\beta}_{1s}}{V_m}\end{aligned} \tag{11}$$

In equation (11), $\bar{q}$ and $\bar{p}$ denote the nondimensional pitch and roll rates, $\dot{\beta}_{1c}$ and $\dot{\beta}_{1s}$ are the rotor longitudinal and lateral flapping rates, χ is the steady wake skew angle, which can be calculated from momentum theory as

$$\chi=\tan^{-1}\left(\frac{\mu}{\lambda_0}\right) \tag{12}$$

and V_m is the mean inflow parameter as defined in equation (3). The wake spacing parameter S defined in equation (11) physically represents the distance traveled at a velocity of V_m during one rotor revolution.

In Ref. 9, the Peters-He finite state inflow model is extended to account for the quasi-steady wake curvature effect as

$$[K]\begin{Bmatrix}\dot{\alpha}_j^r\\ \dot{\beta}_j^r\end{Bmatrix}+[L]^{-1}\begin{Bmatrix}\alpha_j^r\\ \beta_j^r\end{Bmatrix}=\frac{1}{2}\begin{Bmatrix}\tau_n^{mc}\\ \tau_n^{ms}\end{Bmatrix} \tag{13}$$

where the new L-Matrix is given by

$$[L]=\left[[\tilde{L}]+K_{\mathrm{Re}}[C]\right][V]^{-1} \tag{14}$$

In equation (14), $[V]$ is the mass flow parameter matrix and $[\tilde{L}]$ is the original inflow gain matrix developed in Ref.2 and K_{Re} is the wake curvature parameter. The wake curvature effect matrix $[C]$ is given in Ref. 9, for example, when the model is truncated to the 2nd harmonic terms, as

$$[C]=\begin{bmatrix}[0] & \frac{1}{2}[C_{pk}]^T\kappa_c & [0] & \frac{1}{2}[C_{pk}]^T\kappa_s & [0]\\ [C_{pk}]\kappa_c & [0] & [0] & [0] & [0]\\ [0] & [0] & [0] & [0] & [0]\\ [C_{pk}]\kappa_s & [0] & [0] & [0] & [0]\\ [0] & [0] & [0] & [0] & [0]\end{bmatrix} \tag{15}$$

In equation (15), sub-matrix $[C_{pk}]$ denotes the wake curvature inflow coupling matrix and can be computed prior to simulation or can be represented in simulation using a set of pre-trained neural nets (Ref. 11). It can be seen that the gain matrix $[L]$ in equation (14) involves the wake skew X, longitudinal and lateral wake curvatures, κ_c and κ_s, and the mass inflow parameter matrix involving the wake spacing S. Therefore, Equations (9) and (13) together constitute the new dynamic wake model.

In Ref.5, the Pitt-Peters dynamic inflow model is modified to take into account of quasi-steady wake curvature effect as

$$\begin{bmatrix}\frac{128}{75\pi} & & \\ & \frac{16}{45\pi} & \\ & & \frac{16}{45\pi}\end{bmatrix}\begin{Bmatrix}\dot{\lambda}_0\\ \dot{\lambda}_s\\ \dot{\lambda}_c\end{Bmatrix}+[V]\begin{bmatrix}\frac{1}{2} & \frac{K_{\mathrm{Re}}K_s}{2} & \frac{K_{\mathrm{Re}}K_c}{2}-\frac{15\pi}{64}X\\ \frac{K_{\mathrm{Re}}K_s}{2} & 2(1+X^2) & 0\\ \frac{K_{\mathrm{Re}}K_c}{2}+\frac{15\pi}{64}X & 0 & 2(1-X^2)\end{bmatrix}^{-1}\begin{Bmatrix}\lambda_0\\ \lambda_s\\ \lambda_c\end{Bmatrix}=\begin{Bmatrix}C_T\\ -C_L\\ -C_M\end{Bmatrix} \tag{16}$$

Equation (16) also depends on the wake skew, X, longitudinal and lateral wake curvatures, κ_c and κ_s, wake curvature parameter K_{Re}, and the mass flow parameter matrix involving the wake spacing, S. Once again, equations (9) and (16) are solved simultaneously in order to account for dynamic wake distortion effects.

Comparison of Wake Distortion Models

Keller (Ref. 4) proposed a way to represent the quasi-steady wake distortion effect during maneuvering flight. The corresponding augmented Pitt-Peters inflow model can be written as (only the longitudinal case is considered here, the same analysis can be applied to the lateral case)

$$[M]\begin{Bmatrix}\dot{\lambda}_0\\ \dot{\lambda}_c\end{Bmatrix}+[V]\begin{bmatrix}\frac{1}{2} & -\frac{15\pi}{64}X\\ \frac{15\pi}{64}X & 2(1-X^2)\end{bmatrix}^{-1}\begin{Bmatrix}\lambda_0\\ \lambda_c-K_R\bar{q}\end{Bmatrix}=\begin{Bmatrix}C_T\\ -C_M\end{Bmatrix} \tag{17}$$

where K_R is the wake distortion parameter. In equation (17), Keller models the wake curvature effect as additional forcing terms in the original Pitt-Peters dynamic inflow model. Carrying out the matrix inversion in equation (17) and simplifying the resulting equation gives rise to

$$[M]\begin{Bmatrix}\dot{\lambda}_0\\ \dot{\lambda}_c\end{Bmatrix}+\begin{bmatrix}2V_m\lambda_0(1-X^2)-\frac{15\pi X}{64}V_m(\lambda_c-K_R\bar{q}) \\ \frac{15\pi X}{64}\bar{V}\lambda_0+\frac{1}{2}\bar{V}(\lambda_c-K_R\bar{q})\end{bmatrix}\begin{Bmatrix}\lambda_0\\ \lambda_c\end{Bmatrix}=\begin{Bmatrix}C_T\\ -C_M\end{Bmatrix} \tag{18}$$

Where $\bar{V}$ is the inflow parameter with the first harmonic inflow states as defined in equation (2).

On the other hand, the augmented Pitt-Peters dynamic inflow model with steady wake curvature effect in the present study (equation (16)) can be written for the longitudinal case as

$$[M]\begin{Bmatrix}\dot{\lambda}_0\\ \dot{\lambda}_c\end{Bmatrix}+[V]\begin{bmatrix}\frac{1}{2} & \frac{K_{\mathrm{Re}}\kappa_c}{2}-\frac{15\pi}{64}X \\ \frac{K_{\mathrm{Re}}\kappa_c}{2}+\frac{15\pi}{64}X & 2(1-X^2)\end{bmatrix}^{-1}\begin{Bmatrix}\lambda_0\\ \lambda_c\end{Bmatrix}=\begin{Bmatrix}C_T\\ -C_M\end{Bmatrix} \tag{19}$$

It is clear from equation (19) (or equation (16)) that the present study models the wake curvature effect as a modification to the system gain matrix. Equation (19) can be rewritten as

$$[M]\begin{Bmatrix}\dot{\lambda}_0\\ \dot{\lambda}_c\end{Bmatrix}+\begin{bmatrix}2V_m\lambda_0(1-X^2)-\frac{15\pi X}{64}V_m\lambda_c-\frac{K_{\mathrm{Re}}\kappa_c}{2}V_m\lambda_c \\ \frac{15\pi X}{64}\bar{V}\lambda_0+\frac{1}{2}\bar{V}(\lambda_c-K_{\mathrm{Re}}\kappa_c\lambda_0)\end{bmatrix}\begin{Bmatrix}\lambda_0\\ \lambda_c\end{Bmatrix}=\begin{Bmatrix}C_T\\ -C_M\end{Bmatrix} \tag{20}$$

Generally, the perturbations in the total mean inflow λ_0 in equations (18) and (20) are small. Therefore, the equations for the longitudinal inflow gradient appearing in equations (18) and (20) are the same if the following expression is true

$$K_R\bar{q}=K_{\mathrm{Re}}\kappa_c\lambda_0 \tag{21}$$

In Ref. 14, it is shown that the two models near hover are the same provided K_R=K_{Re}. In forward flight case, if the wake curvatures are redefined as

$$(\kappa_c)_{qs}=\frac{\bar{q}-\dot{\beta}_{1c}}{\lambda_0}\quad (\kappa_s)_{qs}=\frac{\bar{p}-\dot{\beta}_{1s}}{\lambda_0} \tag{22}$$

it can be shown from equations (21) and (22) that

$$K_R=K_{\mathrm{Re}} \tag{23}$$

which is the same as the condition for the two models to be consistent with each other near hover as given in Ref. 14. In the remainder of the paper, the modified definition for the wake curvatures as given by equation (22) is used.

In the wake distortion model used in this study, the wake curvatures, κ_c and κ_s, the wake skew X, and the wake spacing S are treated as additional states for inclusion of dynamic wake distortion effects in the model. Similarly, as suggested in Ref. 10, the quasi-steady wake distortion model proposed by Keller (Ref. 4) can be extended to the dynamic wake distortion case by treating the longitudinal and lateral wake distortion effects as additional states.

Simulation Results and Discussion

In Refs. 13 and 14, the dynamic wake distortion model near hover condition is implemented in a generic helicopter flight simulation program (Ref. 16) and simulation results are compared with the flight test data near hover condition to investigate the impact of the dynamic wake distortion effects. In order to evaluate the extended dynamic wake distortion model for forward flight case as developed in this paper, equations (9) and (16) are implemented in the generic helicopter flight simulation program (Ref. 16) and simulation results are compared with the Black Hawk helicopter flight test data (Ref. 17). Likewise, equation (17) with the longitudinal and lateral wake distortion effects as additional states are also implemented in the flight simulation program for the purpose of numerical comparisons between the two wake distortion models.

The Black Hawk helicopter response to a lateral doublet stick input at 40 knots is considered first. Figure 7 shows the stick input profile and Figs. 8 and 9, respectively, show the on-axis (roll rate) and off-axis (pitch rate) response predictions with the two dynamic wake distortion models (Model A: equations (9) and (16); Model B: equation (17) with the longitudinal and lateral wake distortion effects as additional states) to the same lateral cyclic stick doublet of Fig. 7. From Fig. 8, it is seen that dynamic wake distortion has very little effect on on-axis response, which is consistent with previous findings in the literature (Refs. 9, 13, 14). The value of the wake curvature parameter K_{Re} is taken to be 3.8 (same as the value used for the hover case in Refs. 13 and 14). From Fig. 9, it can be seen that the Model A predictions with a wake curvature parameter K_{Re} of 3.8 greatly improves the correlation of off-axis response with flight test data at 40 knots. For comparison purposes, the predicted response without any wake distortion effect (K_{Re}=0) is also shown in Figs. 8 and 9. Also superimposed on Figs. 8 and 9 are the response predictions using Model B with a wake distortion parameter K_R of 3.8. It is clear from these results that both Model A (with a wake curvature parameter of 3.8) and Model B (with a wake distortion parameter of 3.8) give nearly the same on- and off-axis response predictions.

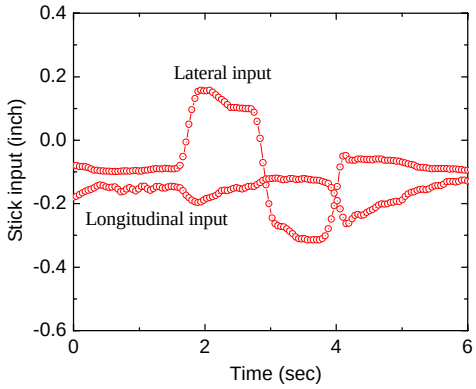

Figure 7. Profile of the lateral cyclic control stick doublet used in the Black Hawk helicopter flight test program at 40 knots.

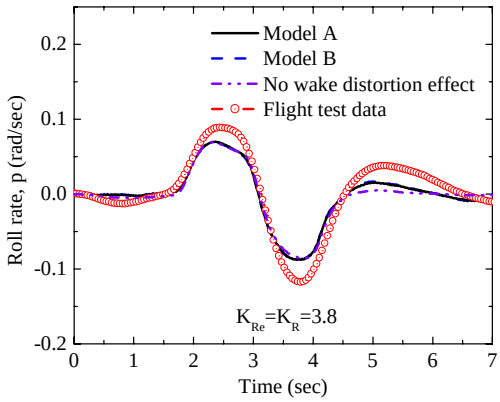

Figure 8. Black Hawk helicopter on-axis (roll rate) response at 40 knots to the lateral cyclic stick doublet of Fig. 7.

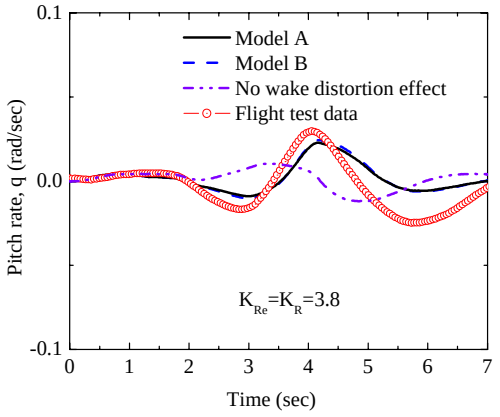

Figure 9. Black Hawk helicopter off-axis (pitch rate) response at 40 knots to the lateral cyclic stick doublet of Fig. 7.

The vehicle response to a longitudinal cyclic control input is considered next. Figure 10 shows the longitudinal cyclic control doublet used in the flight test program. Figures 11 and 12, respectively, show the on-axis (pitch rate) and off-axis (roll rate) responses to the doublet input of Fig. 10. For comparison purposes, predicted responses with and without wake distortion effects are shown along with flight test data in Figs. 11 and 12. Once again, it is seen from Fig. 11 that wake distortion has very little effect on on-axis (pitch rate) response. However, the off-axis (roll rate) response prediction (Fig. 12) is significantly improved with Model A with a wake curvature parameter K_{Re} of 3.8 or with Model B with a wake distortion parameter K_R of 3.8.

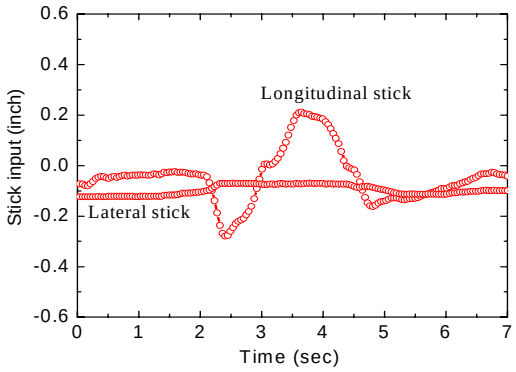

Figure 10. Profile of the longitudinal cyclic control stick doublet used in the Black Hawk helicopter flight test program at 40 knots.

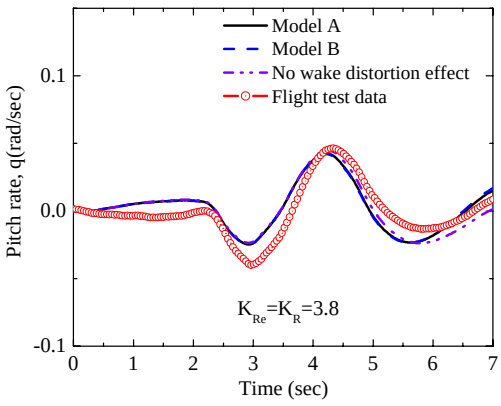

Figure 11. Black Hawk helicopter on-axis (pitch rate) response at 40 knots to the longitudinal cyclic stick doublet of Fig. 10.

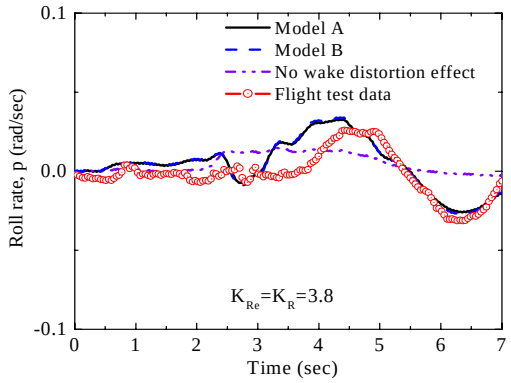

Figure 12. Black Hawk helicopter off-axis (roll rate) response at 40 knots to the longitudinal cyclic stick doublet of Fig. 10.

Conclusions

A reduced order model of wake distortion dynamics for maneuvering and transitioning from forward flight is developed using the vortex tube analysis results. The model is integrated into a generic helicopter flight simulation program and the predicted responses to cyclic control doublets with and without wake distortion effects are compared with the Black Hawk helicopter flight test data at 40 knots. Analytical and numerical comparisons are made between the current model and the augmented dynamic inflow model proposed by Keller et al (Refs. 4, 10). Based on the correlations with flight tests data carried out in this study, the following general conclusions can be made:

1. The proposed dynamic wake distortion model basically captures the right off-axis response at 40 knots to cyclic control inputs.
2. The value of the wake curvature parameter, K_{Re}, is taken to be 3.8, which is the same value used in Refs. 13 and 14 for the hover case. Even with this high value for the wake distortion/curvature parameter used in the present study, there still exist some discrepancies between the simulation predictions and the flight test data at 40 knots. Further work is needed to fully understand the effect of wake distortion/curvature parameter on predicted response.
3. The present study assumes circumferentially uniform vortex strength in the vortex tube analysis, thus capturing the coupling between the inflow gradients and the mean loading only. Further work is needed to model the coupling between inflow gradients and cyclic loading in maneuvering flight.
4. The wake distortion model of the present study and the augmented dynamic inflow model proposed by Keller et al (Refs. 4, 10) are very nearly the same in forward flight case when the wake curvature parameter (K_{Re}) of the present study and the wake distortion parameter (K_R) of the model proposed by Keller et al (Refs. 4, 10) are taken to be equal and the wake curvatures are defined in terms of the rotor total mean inflow.

Acknowledgement

This study was conducted under the US Army/NASA sponsored NRTC Center of Excellence in Rotorcraft Technology program at the Georgia Institute of Technology. The help extended by Dr. Mark Tischler of the Aeroflightdynamics Directorate at the NASA Ames Research Center with the Black Hawk helicopter flight test data is gratefully acknowledged.

References

[1] Pitt, D.M. and Peters, D.A., "Theoretical Prediction of Dynamic Inflow Derivatives," Vertica, Vol. 5, No. 1, pp 21-34, 1981

[2] He, C.J., "Development and Application of a Generalized Dynamic Wake Theory for Lifting Rotors," Ph.D. Thesis, School of Aerospace Engineering, Georgia Institute of Technology, July 1989

[3] Keller, J.D. and Curtiss, H.C., Jr., "Modeling the Induced Velocity of a Maneuvering Helicopter," Proceedings of the American Helicopter Society 52nd Annual Forum, Washington, D.C., June 4-6,1996. pp841-851.

[4] Keller, J.D., "An Investigation of Helicopter Dynamic Coupling Using an Analytical Model," Journal of the American Helicopter Society. Vol.41,(3), July 1995.

[5] Barocela, E., Peters, D.A., Krothapaiil, K.R. and Prasad, J.V.R., "The Effect of Wake Distortion on Rotor Inflow Gradients and Off-Axis Coupling," AIAA paper 97-3559, 1997.

[6] Rosen, A. and Isser A., " A New Model of Rotor Dynamics During Pitch and Roll of a Helicopter", Journal of the American Helicopter Society, Vol.40,(3), July, 1995.

[7] Basset, P.M. and Techen-Fo, F., "Study of the Rotor Wake Distortion Effects on the Helicopter Pith-Roll Cross-Couplings," Proceedings of the 24th European Rotorcraft Forum, Marseilles, France, September 1998.

[8] Bagai, A., Leishman, J.G. and Park, J., "Aerodynamic Analysis of a Helicopter in Steady Maneuvering Flight Using a Free-Vortex Rotor Wake Model," Journal of the American Helicopter Society, April, 1999. Pp 109-120.

[9] Krothapalli, K.R., Prasad, J.V.R. and Peters, D.A., "Helicopter Rotor Dynamic Inflow Modeling for Maneuvering Flight," Journal of the American Helicopter Society, Vol. 46, No. 2, April 2001, pp. 129-139.

[10] Curtiss, H.C. Jr., "Aerodynamic Models and the Off-Axis Response," Proceedings of the American Helicopter Society 55th Annual Forum, Montreal, Canada, May 25-27, 1999.
[11] Prasad, J.V.R., Fanciullo, T., Zhao, J. and Peters, D.A., "Toward a High Fidelity Inflow Model for Maneuvering and In-Ground Effect Flight Simulation," Presented at the American Helicopter Society 57th Annual Forum, Washington DC, May 9-11, 2001
[12] Prasad, J.V.R., Zhao, J. and Peters, D.A., "Modeling of Rotor Dynamic Wake Distortion During Maneuvering Flight," Proceedings of the 2001 AIAA Atmosphere Flight Mechanics Conference, Montreal, Canada, August 6-9, 2001.
[13] Zhao, J., Prasad, J.V.R. and Peters, D.A., "Rotor Dynamic Wake Distortion Model for Helicopter Maneuvering Flight." Presented at the 58th Annual Forum of the American Helicopter Society, Montreal, Canada, 2002.
[14] Zhao, J., Prasad, J.V.R. and Peters, D.A., "Simplified Dynamic Wake Distortion Model for Helicopter Transitional Flight." AIAA-2002-4400, presented at the AIAA Atmospheric Flight Mechanics Conference, Monterey, California, Aug 5-8, 2002.
[15] Drees, J.M.., "A Theory of Airflow through Rotors and its Application to Some Helicopter Problems," Journal of the Helicopter Asociation of Great Britain, Vol. 3, No. 2, 1949.
[16] Howlett, J.J., "UH-60 Black Hawk Engineering Simulation Program, Volume I – Mathematical Model," NASA CR 166309, December 1981.
[17] Abott, W.Y., Benson, J.O., Oliver, R.G. and Williams, R.A., "Validation Flight Test of UH-60A for Rotorcraft Systems Integration Simulator," USAAEFA Project Final Report, No. 79-24, September 1982.